Engineering Fracture Mechanics 272 (2022) 108720

Contents lists available at ScienceDirect

Engineering Fracture Mechanics

journal homepage: www.elsevier.com/locate/engfracmech

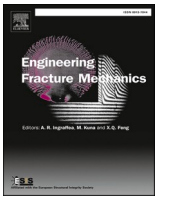

Local creep damage effects on subsequent low temperature fatigue crack growth behaviour of thick-walled pressure vessels

Ali Mehmanparast [a,*], Kamran Nikbin [b]

[a] Department of Naval Architecture, Ocean and Marine Engineering, University of Strathclyde, Glasgow G1 1XQ, UK
[b] Department of Mechanical Engineering, Imperial College London, South Kensington Campus, London SW7 2AZ, UK

A B S T R A C T

The influence of prior creep damage on the subsequent fatigue cracking behaviour of thick-walled pressure vessels has been thoroughly investigated in this study. Creep damage was introduced into fracture mechanics specimens by performing creep tests at 550 °C and stopping them after reaching a desired crack length. Using this experimental methodology, creep damage was successfully introduced ahead of the crack tip in the form of intergranular voids and microcracks. In order to assess the creep damage effects, in the absence of significant plasticity, on the structural integrity of thick-walled pressure vessels the material was uniformly pre-strained under compressive plastic deformation prior to the specimen manufacture, thus hardening the material. Fatigue tests were performed on specimens with and without creep damage and the results were compared with each other. Moreover, metallurgical investigations were conducted to understand the influence of microstructural damages, as a result of creep loading conditions, on the fatigue cracking behaviour of the material. The results from this study show a clear reduction in the fatigue cracking rate in the presence of creep damage local to the crack tip. The findings have been discussed in terms of the effects of static creep loading conditions and microstructural damages on the subsequent fatigue cracking behaviour under cyclic loading conditions.

1. Introduction

Thick-walled pressure vessels are widely used in high temperature applications such as power plants. These high temperature components are often expensive to manufacture and are designed to operate for an extended period of time, which is typically a few decades long. Due to the safety critical applications and limited access to these pressure vessels during the operation phase, it is extremely important to accurately predict the lifetime of such components with suitable safety margins against failure [1]. Therefore, substantial efforts must be put into the design and structural integrity assessment of these high temperature components to avoid unexpected catastrophic failures which can result in radiation disasters. This is the motivation for comprehensive studies on the material's behaviour in high temperature pressure vessels, employed in power plants, which can be subjected to various loading conditions during their operational life cycle.

An important issue that needs to be considered in the structural integrity assessment of high temperature pressure vessels is the influence of prior creep damage on the subsequent fatigue crack growth (FCG) behaviour of the material. In order to take into account this important consideration in the life assessment of high temperature components, it is important to understand and consider the material pre-straining and damage formation process during the following phases:

(i) Global plastic pre-straining during the fabrication phase: Global plastic pre-straining often occurs during the fabrication phase of pressure vessels where the employed manufacturing and forming processes introduce plastic deformations, in the form of tensile and compressive strains, in different parts of the component. Previous studies have shown that plastic pre-straining significantly

* Corresponding author.
E-mail address: ali.mehmanparast@strath.ac.uk (A. Mehmanparast).

https://doi.org/10.1016/j.engfracmech.2022.108720
Received 15 March 2022; Received in revised form 2 June 2022; Accepted 7 August 2022
Available online 13 August 2022

Nomenclature

a	Instantaneous crack length
a_c	Crack length at the end of interrupted creep test
a_f	Final crack length at the end of fatigue test
a_i	Initial crack length at the beginning of fatigue test
Δa	Crack extension
da/dN	Fatigue crack growth rate
B	Total thickness
B_e	Effective thickness
B_n	Net thickness between the side-grooves
C	Paris-law coefficient
C_e	Elastic compliance
C^*	Creep fracture mechanics parameter
E_M	Effective Young's modulus
H	Geometry dependent constant
I_n	Non-dimensional constant
K	Stress intensity factor
K_{max}	Stress intensity factor at maximum load in a fatigue cycle
K_{min}	Stress intensity factor at minimum load in a fatigue cycle
ΔK	Stress intensity factor range
m	Paris-law exponent
n	Power-law creep stress exponent
N	Number of cycles in fatigue test
P	Applied load
P_{max}	Maximum load in a fatigue cycle
P_{min}	Minimum load in a fatigue cycle
P_{LC}	Plastic collapse load for an elastic-perfectly plastic material
r	Radial distance from the crack tip
R^2	Coefficient of determination
t	Time
W	Specimen width
Y	Shape function
σ	Applied stress
σ_0	Normalising stress
σ_{max}	Maximum stress in a fatigue cycle
σ_{min}	Minimum stress in a fatigue cycle
σ_{ref}	Reference stress
$\sigma_{0.2}$	0.2% proof stress (often taken as the yield stress)
$\widetilde{\sigma}_{ij}$	Non-dimensional stress value
$\Delta\sigma$	Stress range
$\dot{\varepsilon}$	Strain rate
$\dot{\varepsilon}_0$	Normalising strain rate
$\widetilde{\varepsilon}_{ij}$	Non-dimensional strain value
θ	Crack tip angle
$\dot{\Delta}$	Load line displacement rate
η	Geometry dependent constant
AGR	Advanced Gas-cooled Reactor
AR	As-Received material state
CCG	Creep Crack Growth
C(T)	Compact Tension specimen geometry
EDM	Electrical Discharge Machining technique
FCG	Fatigue Crack Growth
LCD	Local Creep Damage
LLD	Load Line Displacement
PC	Pre-Compressed material state
PD	Potential drop crack growth monitoring technique
SEM	Scanning Electron Microscope
SS	Stainless Steel

alters the mechanical, creep crack growth (CCG) and fracture behaviour of high temperature pressure vessels [2-5]. Therefore, the extent of plastic pre-strains, which are formed during the fabrication processes, must be accurately identified and considered in the structural integrity assessment of high temperature components.

Some work has been previously conducted by other researchers to examine the plastic pre-straining effects on the fatigue life and crack growth behaviour of engineering materials. For example, it has been shown in [6] that plastic pre-straining effects were relatively minor in 304L stainless steel when uniaxial fatigue tests were conducted under strain-control mode. It has been reported in [6] that in load-control mode some effects were found in the low cycle region whereas extended lives were obtained in the high cycle region. It has been shown in [7] that at high strain amplitudes, the fatigue behaviour of the cold worked 316L(N) stainless steel was found similar to the as-received (AR) condition; however, longer fatigue lives were found in the cold worked material state at lower strain amplitudes. Furthermore, the test results on stainless steel and mild steel specimens in [8,9] have shown that the fatigue crack propagation rate decreased by increasing the pre-straining level. A similar deceleration in the FCG rate of a low carbon steel with increasing the percentage of pre-strain has also been reported in [10]. Finally found in the literature is that the plastic pre-strain led to a small reduction in the fatigue crack propagation rate of Al-alloy 6061-T6 [11].

(ii) Global creep pre-straining during the operation phase: In addition to plastic pre-strains, which may appear during the fabrication phase, the global creep pre-strains start to form during the operation phase of the high temperature components. This is due to the constant exertion of operational forces on the pressure vessels at elevated temperature which would introduce time-dependent creep pre-straining into the material. Previous investigations have revealed that similar to plastic pre-straining, global creep pre-straining also changes the mechanical and fracture behaviour of high temperature components [12,13]. Hence, the influence of global pre-straining, which is generally referred to as inelastic pre-straining in the presence of combined plastic and creep pre-strains, must be considered in integrity management of high temperature pressure vessels.

The influence of global creep pre-strains on the fatigue resistance of CrMoV was examined in [14]. It was found that prior creep strain had detrimental effects on the fatigue resistance of the material. Also shown and discussed in [14] is that the applied stress, testing temperature, and creep ductility play key roles in the subsequent fatigue life of the material. The influence of global creep pre-strains on the subsequent tensile and fracture behaviour of 316 stainless steel was investigated in [15]. It has been reported in [15] that the creep pre-strain material state exhibited a moderate increase in the yield stress, severe reduction in tensile strain at failure and a rapid drop in the fracture energy (found by Charpy tests) compared to the AR material state. These experimental observations are consistent with those reported on Type 316H SS in [13,16].

(iii) Creep damage during the operation phase: While the global creep pre-straining has been found to harden the material by increasing the yield stress and decreasing the tensile strain at failure, the operational loads could eventually result in material degradation and damage which would appear by initiation of creep cracks that will continue to propagate under static creep loads. Under these conditions, creep damage forms in a confined space ahead of the crack tip which is generally referred to as local creep damage (LCD) and is featured by intergranular voids and microcracks that can link up to form macrocracks ahead of the main crack tip. Although extensive studies have been performed in the past decade to better understand the influence of global plastic and creep pre-strains on the asset integrity management of high temperature components, the influence of LCD is yet to be understood.

An important industrial application, which motivates the need for further research on the LCD effects, is the life-extension and structural integrity assessment of the high temperature pressure vessels in the UK's advanced gas-cooled reactors (AGRs). Some of these thick-walled pressure vessels, which are widely made of Type 316H stainless steel (SS), have previously operated in the creep regime at elevated temperatures and subsequently had their operating temperatures reduced for life-extension purposes. This means that while creep cracks might have formed in these aged high temperature components, the propagation behaviour of the pre-existing creep cracks must be carefully characterised at lower temperatures. One of the most important failure mechanisms in the aged AGRs after temperature reduction is FCG due to the cyclic loading conditions applied on the aged and creep cracked pressure vessels as a result of power ups and shut downs. Therefore, there is an essential need to investigate the influence of prior LCD effects on subsequent FCG behaviour of the materials which has not been yet investigated in any research study. This information helps to improve the current procedures for the life prediction of aged pressure vessels employed in high temperature applications.

In this study, the LCD has been introduced into fracture mechanics specimens by performing CCG experiments at an elevated temperature and interrupting the tests upon reaching a desired extent of crack propagation. Subsequently, FCG tests have been performed on the LCD specimens to investigate the influence of creep damage, local to the crack tip, on the fatigue crack propagation behaviour of the material. Post-mortem analysis has been conducted to explore the microstructural features and cracking mode under creep and fatigue loading conditions. The results from this study have been discussed in terms of the mechanical and microstructural effects of LCD on the fatigue cracking behaviour of the high temperature pressure vessels.

2. Specimen geometry and preparation process

In the present study, an ex-service steam header (i.e. pressure vessel) made of Type 316H stainless steel was provided by EDF Energy and used in experimental investigations. The mechanical and creep properties of the ex-service material were previously characterised by the authors in a separate study [2]. The material characterisation results in [2] showed that Type 316H SS has a relatively low yield stress of $\sigma_y \approx 170$ MPa at 550 ℃, which is the typical operational temperature for steam headers in AGRs. Knowing that in a cracked geometry the plastic zone size ahead of the crack tip is inversely proportional to the yield stress of the material [17], this means that during CCG tests on the AR 316H SS at 550 ℃ significant level of plasticity will form ahead of the crack tip. This implies that the interpretation of the obtained results from CCG tests on AR 316H SS at 550 ℃ would be complicated due to the difficulties to distinguish between the creep damage and plasticity effects on the cracking behaviour of the material. For the purpose of the present

study, which is to investigate the creep damage effects on FCG, it was decided to eliminate the plastic deformation ahead of the crack tip by globally pre-straining the material prior to CCG testing. It has been previously shown that global plastic pre-straining hardens the material (i.e. increases the yield stress) [2]. Therefore, the material was globally pre-strained before CCG testing to reduce the plastic deformation ahead of the crack tip during the creep tests.

Blocks of 316H SS were initially extracted from the ex-service steam header and then uniformly pre-compressed (PC) to 8% plastic strain at room temperature. The mechanical and creep properties of the PC material were previously characterised and compared with the AR material state in [2]. After completion of material pre-straining process, compact tension, C(T), specimens were extracted from the pre-compressed blocks. The C(T) specimens were extracted with the loading axis parallel to the pre-straining direction.

Five C(T) specimens were manufactured from the pre-strained blocks. In order to prepare LCD specimens, interrupted CCG tests were performed on two of the extracted specimens from the pre-compressed (PC) material (denoted LCD1 and LCD2). Once creep damage was introduced into these two specimens, FCG tests were performed to examine the LCD effects on the fatigue crack propagation behaviour of the material. In order to compare the FCG behaviour in the presence and absence of creep damage, another three tests (denoted FCG-PC1, FCG-PC2 and FCG-PC3) were carried out on C(T) specimens manufactured from the PC blocks. Moreover, three additional FCG tests were performed on the AR material state (denoted FCG-AR1, FCG-AR2 and FCG-AR3) for comparison purposes to evaluate the global plastic pre-straining effects on the FCG behaviour of the material.

All C(T) specimens were designed and tested in accordance with ASTM E647 standard [18]. The C(T) specimens had the width of $W = 50$ mm, thickness of $B = 25$ mm and net thickness between the side-grooves of $B_n = 17.5$ mm. The starter crack in LCD specimens was introduced using the Electrical Discharge Machining (EDM) technique with the notch root radius of 0.125 mm. The AR and PC specimens were pre-fatigue cracked using the decreasing ΔK approach to introduce sufficiently sharp crack tip into the test specimens. The interrupted CCG tests on LCD specimens were performed at 550 °C while all FCG tests were conducted at room temperature for simplicity. In this paper, the test results from the AR, PC and LCD specimens are shown in red, blue and green symbols, respectively.

3. Creep damage and fatigue crack growth testing and analysis

3.1. Local creep damage tests

3.1.1. Creep testing procedure and loading conditions

In order to introduce creep damage into the material, local to the crack tip, interrupted CCG tests were carried out on two C(T) specimens, manufactured from the PC material, following the procedure described in ASTM E1457 standard [19]. The CCG tests on LCD1 and LCD2 specimens were started at the initial normalised crack length of $a_0/W = 0.35$ (i.e. $a_0 = 17.5$ mm) and stopped when the normalised crack length reached a desired value of around $a/W \approx 0.5$ (i.e. $a \approx 25$ mm). In order to interrupt the CCG tests on LCD specimens at the desired crack length, two calibration tests were initially conducted on nominally identical C(T) specimens (denoted 8PC-A2 and 8PC-A3) extracted from the same steam header and with the same plastic pre-strain level as the LCD specimens. These two calibration CCG tests were subjected to a load level corresponding to the stress intensity factor of $K(a_o) = 25.5$ MPa$\sqrt{\text{m}}$ at the beginning of the tests. The crack growth monitoring in the calibration tests was performed using the potential drop (PD) technique and the output voltage values were continuously recorded throughout the tests. Upon completion of the calibration CCG tests, the specimens were broken open to measure the final crack length using the optical imaging technique on the fracture surface. The initial and final crack lengths were measured and used to calibrate the PD data, and convert the voltage values into crack lengths. The calibrated PD data from these two tests on 8PC-A2 and 8PC-A3 specimens were used to interrupt the tests on LCD specimens, which were conducted under the same load level, at the desired crack length of $a/W \approx 0.5$ (see Fig. 1).

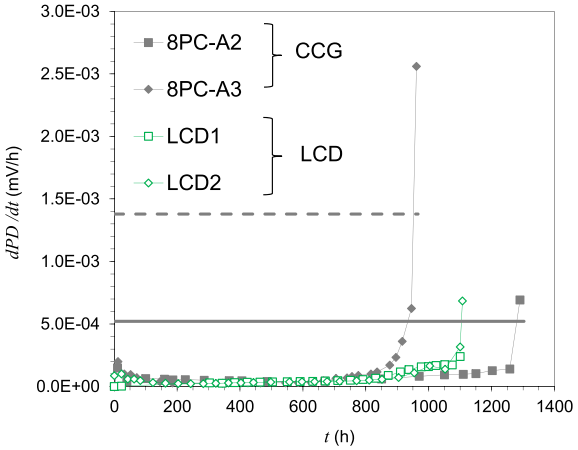

Fig. 1. Comparison of the PD rates in LCD specimens and calibration CCG tests.

3.1.2. Interruption of creep crack growth tests at a desired crack length

A comparison of the variation in PD rates (dPD/dt) over time in LCD specimens (shown in green symbols) and the calibration CCG tests (shown in solid grey symbols) is illustrated in Fig. 1. Also seen in these figures are the grey solid and dashed lines to indicate the values of dPD/dt at $a/W = 0.5$ in 8PC-A2 and 8PC-A3 calibration CCG tests, respectively. As seen in Fig. 1, different PD rates have been obtained from 8PC-A2 and 8PC-A3 tests at the a/W of 0.5. This difference in the PD rates can be attributed to a number of factors particularly the exact probe location which might be slightly different in two specimens [20]. It is worth noting that accelerated CCG rates are observed in the PC 316H material, compared to the AR condition. This means that at larger crack lengths a significant increase in the PD rates occurred in a relatively short period of time during the tests on PC material. Therefore, the CCG tests on LCD specimens were interrupted at the earliest convenient time when a PD rate of close to or between those corresponding to $a/W = 0.5$ in 8PC-A2 and 8PC-A3 tests was achieved. As seen in Fig. 1, LCD2 test was stopped at the PD rate of around 5×10^{-4} (mV/h) which corresponds to the $a/W = 0.5$ in the CCG test on 8PC-A2 sample. However, LCD1 test was stopped at a lower PD rate. The measured creep crack lengths at the end of the CCG tests on LCD specimens, a_c, are summarised in Table 1. Also seen in Table 1 are the values of the stress intensity factor, $K(a_c)$, at the points that CCG tests on LCD specimens were stopped. As seen in this table, the interruption of the CCG tests on LCD specimens at the expected PD rates obtained from calibration tests was very successful and the LCD1 and LCD2 tests were stopped at a normalised crack length of very close to $a/W = 0.5$.

3.1.3. Estimation of the extent of plasticity in local creep damage specimens

As explained earlier, the creep damage tests were performed on specimens extracted from the PC material which had a higher yield stress and smaller plastic zone size ahead of the crack tip compared to the AR condition. The CCG tests on LCD specimens were performed under the same loading condition as the calibration tests (with $K(a_o) = 25.5$ MPa$\sqrt{\text{m}}$). In order to evaluate the level of plasticity in the LCD specimens, the reference stress σ_{ref} approach was employed in the analysis. It has been shown and explained in [21] that the ratio of reference stress over 0.2% proof stress (i.e. which is often taken as the yield stress for the ductile materials), $\sigma_{ref}/\sigma_{0.2}$, indicates the level of plasticity in a cracked geometry and can be defined as:

$$\frac{\sigma_{ref}}{\sigma_{0.2}} = \frac{P}{P_{LC}} \tag{1}$$

where P is the applied load and P_{LC} is the plastic collapse load for an elastic-perfectly plastic material, the solutions of which are provided in [17]. If the normalised reference stress is much larger than unity, it implies that there is widespread plasticity in the specimen. If this ratio is much less than unity, a limited amount of plasticity is expected in the cracked geometry. As seen in Table 2, the values of normalised reference stress in LCD specimens at a/W of 0.35 and 0.5 are both much smaller than unity, indicating limited extent of plasticity ahead of the crack tip. This allowed the influence of prior creep damage on subsequent FCG behaviour of the material to be investigated in the absence of significant plastic deformation at the crack tip.

3.2. Fatigue crack growth tests

3.2.1. Cyclic loading conditions

FCG tests were performed on three AR (FCG-AR1, FCG-AR2, FCG-AR3), three PC (FCG-PC1, FCG-PC2, FCG-PC3) and two LCD (LCD1 and LCD2) specimens following the procedure described in ASTM E647 [18]. Prior to FCG testing, the AR and PC specimens were pre-fatigue cracked from the initial machined notch length of $a_0/W = 0.35$ (i.e. $a_0 = 17.5$ mm) to $a/W \approx 0.5$ (i.e. $a \approx 25$ mm). Subsequently, the main fatigue tests were performed using a sinusoidal waveform under constant amplitude loading conditions, where the maximum load P_{max} and minimum load P_{min} were kept constant throughout the tests. Due to the necessity of side-grooving in interrupted CCG tests on LCD1 and LCD2 specimens (see the recommended specimen design guidelines in ASTM E1457 standard [19]), the specimens made of the AR and PC materials states were also side-grooved for direct comparison with LCD specimens. All FCG tests were conducted at a load ratio of $R = 0.1$, where R is the ratio of P_{min} over P_{max} in a fatigue cycle, and frequency of $f = 10$ Hz. For the AR and PC specimens, the fatigue tests were conducted under the contact loads of $P_{max} = 9.7$ kN and $P_{min} = 0.97$ kN, which were corresponding to the initial stress intensity factor range of $\Delta K = 18.5$ MPa$\sqrt{\text{m}}$ at the beginning of the tests. The FCG test on LCD1 specimen was initially started under the same loading conditions as the AR and PC materials. However, no crack growth was observed after an extended period of time, thus the load values were increased to $P_{max} = 14.6$ kN and $P_{min} = 1.46$ kN, which were corresponding to the initial stress intensity factor range of $\Delta K = 23.5$ MPa$\sqrt{\text{m}}$ at the beginning of the test. The FCG test on LCD2 specimen was conducted under the same cyclic load levels as LCD1 specimen.

Table 1
Creep crack length measurements and the stress intensity factor in LCD specimens.

Test ID	a_c (mm)	$K(a_c)$ (MPa$\sqrt{\text{m}}$)
LCD1	24.7	37.0
LCD2	26.6	41.8

Table 2
The values of the normalised reference stress at the beginning and end of the interrupted CCG tests.

a/W	$K(a_0)$ (MPa$\sqrt{m}$)	σ_{ref} / $\sigma_{0.2}$
0.35	25.5	0.33
0.5	40.2	0.70

3.2.2. Crack growth monitoring

The crack growth monitoring in FCG tests was carried out using the unloading compliance techniques. For this purpose, a clip gauge was accurately calibrated and accommodated at the crack mouth of the C(T) specimens to measure the change in the load line displacement (LLD) throughout the tests. Using the LLD data, the instantaneous crack lengths in FCG tests were estimated using the unloading compliance technique, similar to the methodology specified in ESIS P2-92 [22] and ASTM E1820 [23] for fracture toughness testing. According to the guidelines provided in these standards, the crack length in fracture mechanics specimens can be estimated, with high accuracy, by:

$$a/W = \begin{pmatrix} 1.000196 - 4.06319\mu + 11.242\mu^2 \\ -106.043\mu^3 + 464.335\mu^4 - 650.677\mu^5 \end{pmatrix} \quad (2)$$

where a is the instantaneous crack length, W is the specimen width and μ is calculated using:

$$\mu = \frac{1}{\sqrt{B_e E_M C_e} + 1} \quad (3)$$

In Eq. (3), C_e is the elastic unloading compliance calculated using the LLD data captured by the clip gauge, E_M is the effective Young's modulus which can be calculated using the equation given in fracture toughness standards [22,23], and B_e is the effective thickness which can be calculated using:

$$B_e = B - (B - B_n)^2 / B \quad (4)$$

where B is the total thickness and B_n is the net thickness between the side grooves.

3.2.3. Crack length measurements on the fracture surface

Upon completion of the FCG tests, the specimens were initially heat tinted and then broken open to measure the initial and final crack lengths on the fracture surface using the optical imaging technique (see [24] for further methodology details). The specimen dimensions, the initial crack length, a_i, the final crack length, a_f, and the crack extension, Δa, in all FCG test specimens are summarised in Table 3. It is worth noting that for LCD specimens the initial fatigue crack length, a_i, was the same as the final crack length at the end of the interrupted CCG tests, a_c. Also included in Table 3 is the comparison of the initial and final crack length values measured on the fracture surface with those estimated from the unloading compliance technique. As seen in this table, the unloading compliance technique has been found to provide accurate estimates of the initial and final crack lengths with relatively low percentage of error. This observation confirms that reliable estimates of the instantaneous crack length were obtained from the unloading compliance measurements throughout the FCG tests on the AR, PC and LCD specimens.

3.2.4. Fatigue crack growth data analysis

In the early 1960 s, it was shown by Paris that the FCG behaviour of engineering materials can be characterised using the fracture mechanics parameters [25,26]. Since then, fracture mechanics have been widely applied to describe the FCG behaviour of materials. The FCG data is usually plotted in the form of crack propagation rate, da/dN, against the change in stress intensity factor, ΔK, in log–log axes. The FCG curves, in general, exhibit a near threshold region (i.e. primary region), followed by a steady state region (i.e. secondary region), and finally an accelerated cracking region (i.e. tertiary region) [17]. In FCG analysis, the minimum value of ΔK at the

Table 3
Fatigue crack growth specimen dimensions.

Test ID	W (mm)	B (mm)	B_n (mm)	P_{max} (kN)	P_{min} (kN)	a_i (mm)	a_f (mm)	Δa (mm)	a_i (mm)	a_f (mm)	% Error	
						Measured			Estimated		a_i	a_f
FCG-AR1	50.0	25.0	17.5	9.7	0.97	26.2	37.6	11.4	25.0	37.8	4.7	0.4
FCG-AR2	50.0	25.0	17.5	9.7	0.97	25.9	37.4	11.5	25.0	37.7	3.5	0.8
FCG-AR3	50.0	25.0	17.5	9.7	0.97	26.1	35.0	8.9	25.6	35.0	2.0	0.0
FCG-PC1	50.0	25.0	17.5	9.7	0.97	25.5	37.9	12.4	25.0	37.9	2.1	0.1
FCG-PC2	50.0	25.0	17.5	9.7	0.97	25.6	37.8	12.2	25.0	38.4	2.3	1.7
FCG-PC3	50.0	25.0	17.5	9.7	0.97	25.6	34.5	8.9	24.7	35.13	3.4	1.8
LCD1	50.0	25.0	17.5	14.6	1.46	24.7	34.1	9.4	–	34.9	–	2.5
LCD2	50.0	25.0	17.5	14.6	1.46	26.6	36.8	10.2	–	33.9	–	7.9

beginning of the threshold region below which a pre-existing crack doesn't start to propagate under cyclic loading conditions is referred to as the threshold stress intensity factor range value, ΔK_{th}. According to the Paris-law, the crack growth rate, da/dN, in the secondary (i.e. steady state) FCG region can be correlated with the fracture mechanics parameter ΔK using a power-law relationship [25]:

$$\frac{da}{dN} = C\Delta K^m \tag{5}$$

where C and m are empirical material constants which can be found using a regression fit to the test data in the secondary FCG region. It has been shown in various studies that the constant m generally ranges between $2 < m < 7$ [17]. It is worth noting that in the present study, da/dN calculations were conducted using the seven-point polynomial technique which provides more accurate calculations compared to the secant method [27]. In Equation (5), the stress intensity factor range ΔK for a given crack length, a, can be described as:

$$\Delta K = K_{max} - K_{min} = \Delta\sigma Y\sqrt{a} \tag{6}$$

where K_{max} and K_{min} are the stress intensity factor values corresponding to P_{max} and P_{min}, respectively, $\Delta\sigma$ is the difference between the maximum stress σ_{max} and minimum stress σ_{min}, and Y is a non-dimensional shape function, the solutions of which for a wide range of cracked geometries can be found in [28].

4. Fatigue crack growth test results

4.1. Variation of the crack length against number of cycles

The variation of the crack length, a, which has been estimated from the unloading compliance data is plotted against the number of cycles, N, for the FCG tests performed on the AR and PC materials in Fig. 2(a). Comparison of the FCG trends for the AR and PC specimens, which all had the same dimensions and were tested under identical cyclic loading conditions, shows that for the first half of the test duration similar cracking behaviour can be observed in the AR and PC material states. However, in the second half of the test duration (i.e. $N > 4.0 \times 10^4$) for a given value of N slightly larger extent of crack length can be observed in the AR material compared to the PC material. Further seen in Fig. 2(a) is that an accelerated FCG behaviour is exhibited towards the end of the tests in the AR and PC specimens. The variation of the crack length estimated from the unloading compliance plotted against the number of cycles for the FCG tests on LCD1 and LCD2 specimens is illustrated in Fig. 2(b). As see in this figure, unlike the tests on the AR and PC specimens, a substantial delay in crack initiation and early-stage fatigue crack propagation can be observed in LCD1 and LCD2 specimens, particularly in LCD1 specimen in which no noticeable crack propagation was observed in the first half of the test. Knowing that the extent of plasticity ahead of the crack tip is limited in LCD specimens (see Section 3.1.3), the delayed crack propagation in LCD specimens can be associated with the strain hardening effects due to widespread creep deformation ahead of the crack tip. This will be explained in more details in the discussion section.

4.2. Variation of the stress intensity factor against number of cycles

The variation of the maximum stress intensity factor, K_{max}, against the crack length for the FCG tests performed on AR, PC and LCD specimens is illustrated in Fig. 3. As seen in this figure, the observed trends for the AR and PC specimens fall on top of each other and for

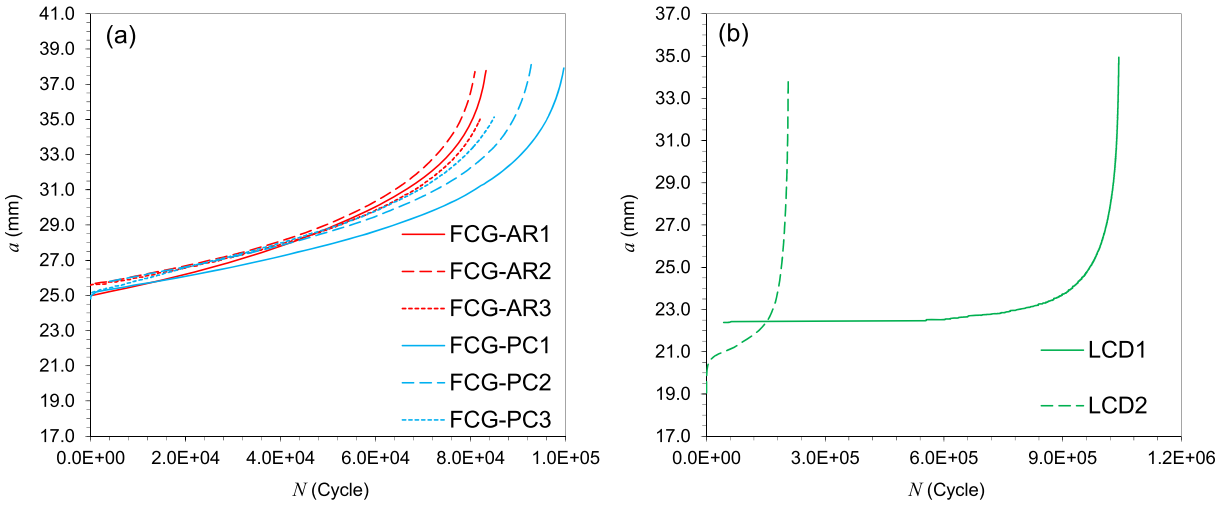

Fig. 2. The variation of the crack length against the number of cycles for (a) AR and PC, and (b) LCD specimens.

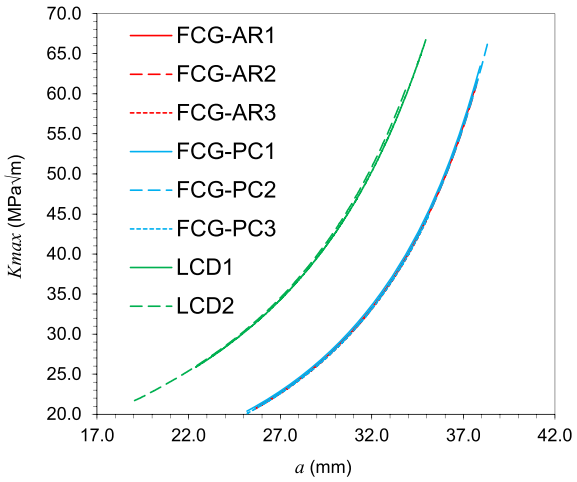

Fig. 3. The variation of the maximum stress intensity factor K_{max} against the crack length for the AR, PC and LCD specimens.

a given value of the crack length, greater K_{max} values can be observed in LCD specimens compared to the AR and PC samples. This is due to the higher initial ΔK value applied in the fatigue tests on LCD specimens (see Section 3.2.1). Also seen in Fig. 3 is that the initial K_{max} value applied on LCD specimens was severely lower than that previously applied at the end of the interrupted CCG tests (see Table 1). The lower loads during cyclic tests on LCD specimens, compared to CCG loading conditions, were maintained to avoid introducing additional inelastic pre-straining and damage into the material. In other words, the lower loads in FCG tests on LCD specimens ensured that the prior creep damage and widespread creep deformation ahead of the crack tip will not be washed out by applying a higher load, hence the LCD effects on the subsequent FCG behaviour of the material can be investigated in these experiments.

4.3. Plastic pre-straining effects on fatigue crack growth behaviour

The FCG rate, da/dN, has been correlated with the stress intensity factor range, ΔK, in Fig. 4(a) and Fig. 4(b) for the tests performed on the AR (FCG-AR1—3) and PC (FCG-PC1—3) specimens, respectively. The results in Fig. 4 are plotted in log–log axes and the da/dN data have the unit of mm/Cycle. As seen in Fig. 4, the FCG data for the AR and PC specimens appear as a straight line with similar trends when presented in log–log axes. The lines of best fits have been made to each data set, within the steady state Paris region, and the FCG power-law constants obtained from these regression fits are summarised in Table 4. Also included in this table are the R^2 values which indicate the accuracy of each line of best fit, hence the level of scatter in the test data. As seen in Table 4, all R^2 values are close to unity and thus acceptable fits with minimum level of scatter have been obtained from these test data. Table 4 shows that the

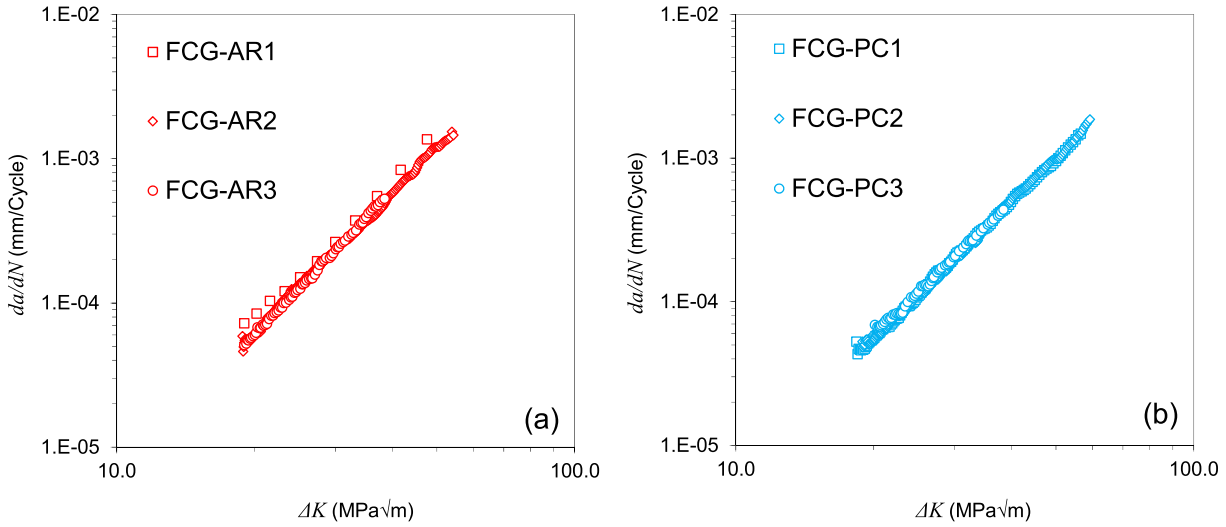

Fig. 4. Correlation of the crack growth per cycle with the stress intensity factor range for the FCG tests performed on the (a) AR, and (b) PC specimens.

Table 4
Fatigue crack growth power-law constants for AR and PC material states.

Test ID	C	m	R^2
FCG-AR1	5.34×10^{-9}	3.20	0.99
FCG-AR2	4.27×10^{-9}	3.20	0.99
FCG-AR3	3.04×10^{-9}	3.30	0.99
FCG-PC1	4.09×10^{-9}	3.17	0.99
FCG-PC2	3.73×10^{-9}	3.20	0.99
FCG-PC3	4.97×10^{-9}	3.12	0.99

FCG power-law coefficient, C, and exponent, m, are almost the same in both AR and PC materials ($C = 4 \pm 1 \times 10^{-9}$ and $m = 3.2 \pm 0.1$). Fig. 4 and Table 4 show that although slightly lower FCG trends may be inferred in the PC material compared to the AR, the global pre-straining process may be considered to have insignificant effects on the FCG behaviour of the material.

4.4. Creep damage effects on fatigue crack growth behaviour

The FCG data from LCD specimens are compared with the mean fits made to the AR and PC data in Fig. 5. Note that for ΔK calculations, the accurate solutions of Y, which are valid for a wide range of a/W values, were taken from ASTM E647 standard [18] and employed in the analysis. As mentioned earlier, sufficiently sharp transgranular crack tips were introduced into the AR and PC specimens by pre-fatigue cracking them before FCG testing. Therefore, the FCG behaviour of the AR and PC materials can be described using the K fracture mechanics parameter [21]. Knowing that microcracks and unbroken ligaments are present at the crack tip in LCD specimens, K parameter may still be employed to characterise the FCG behaviour of the LCD specimens by assuming that the existing creep cracks at the beginning of the tests on LCD specimens are also sufficiently sharp.

As seen in Fig. 5, significantly lower FCG rates of around two orders of magnitude smaller than those observed in the AR and PC material states were obtained in LCD1 and LCD2 specimens at the early stage of the FCG tests. However, as the crack propagates and the value of ΔK increases, the FCG trends for both LCD specimens converge with the mean fits made to the AR and PC material states. This implies that due to the existence of creep damage ahead of the crack tip in LCD specimens, the da/dN values are initially lower than the PC material with no creep damage. However, when the crack advances and the crack tip is located outside the creep damage zone, the FCG behaviour of LCD specimens gets similar to the PC material. Comparison of the FCG behaviour of both LCD specimens with PC specimens shows that the magnified threshold behaviour in LCD1 and LCD2 specimens is due to the high values of creep pre-strains at the crack tip which would harden the material local to the crack tip and decelerate the FCG rates at the early stages of the test [29,30]. Similar declaration in the FCG rate has been reported by other researchers when local plastic pre-strains were introduced to the region ahead of the crack tip [31-34]. Therefore, the results from this study show that the creep damage ahead of the crack tip has a similar effect as the local plastic pre-strains, and they both reduce the FCG rates.

It can be seen in Fig. 5 that similar trends have been obtained from the FCG tests on LCD1 and LCD2 specimens; however, the early stage ΔK values for LCD2 are slightly greater than LCD1. This is due to the fact that under the same cyclic load levels applied on both specimens (i.e. $P_{max} = 14.6$ kN and $P_{min} = 1.46$ kN), LCD2 specimen which had a greater initial crack length compared to LCD1 (see Table 1) has exhibited a higher value of ΔK at the beginning of the FCG test. It can be seen in Fig. 5 that after the first millimetres of crack extension in LCD2 specimen, the FCG data follow the same trend exhibited by LCD1. This implies that despite small differences in the early stage FCG behaviour, due to the microstructural damages as a result of prior creep condition, good repeatability can be observed in the fatigue tests on creep damaged specimens.

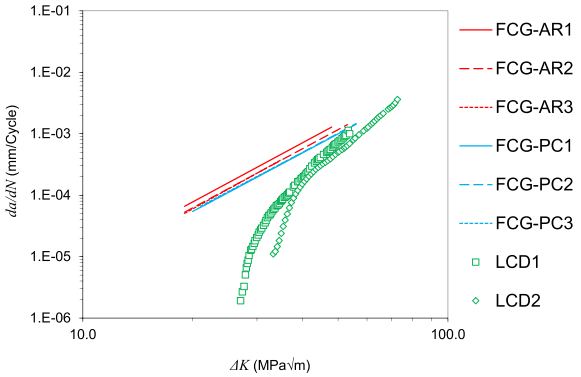

Fig. 5. Comparison of the FCG trends for the AR, PC and LCD specimens.

5. Fractography

In order investigate the fatigue cracking mode in the presence of creep damage, a 3 mm section was sliced from the mid-thickness of the LCD1 specimen for metallography analysis prior to the specimen break open. The sectioned slice was ground, polished and electro-etched using 10% Perchloric Acid in Methanol electrolyte at −20 °C. The prepared section was examined under a Scanning Electron Microscope (SEM) to investigate the crack growth behaviour under creep and fatigue loading conditions. The macro-scale cracking mode in LCD1 specimen is demonstrated in Fig. 6 with the transition region between CCG and FCG regions bounded in a box and shown in a higher magnification for more detailed analysis. Also shown in Fig. 6 are the extents of crack growth under CCG and FCG loading conditions which were measured on the fracture surface after the specimen break open.

As seen in Fig. 6, under static CCG loading conditions the macro-scale cracking mode is intergranular with the crack growth occurring along the grain boundaries, whereas transgranular crack growth can be observed under FCG cyclic loading conditions. At the intermediate region (see the higher magnification SEM image in Fig. 6), an interaction between CCG and FCG failure mechanisms occurs. Therefore, as seen in Fig. 6 a combined intergranular-transgranular cracking behaviour can be observed at the early stage of FCG region. This is due to the existence of voids and microcracks along the grain boundaries due to the prior creep damage in the transition region. As a result of creep damage formation, while the fatigue cracking tends to be transgranular, the pre-existing damage on the grain boundaries introduces stress concentrations and causes the tendency towards diverged cracking as opposed to straight and transganular cracking which is expected to happen under cyclic loading conditions. This diverged cracking phenomenon, which will be more pronounced if the grain boundary forms a larger angle with respect to the naturally preferred straight line for fatigue cracking, makes the switch over from intergranular creep to transgranular fatigue cracking more challenging and slows down the subsequent FCG behaviour in the creep damage zone. As seen in Fig. 6, dominantly transgranular fatigue cracking mode can be observed further away from the creep damage zone where the intergranular damage slowly fades away.

In addition to the cracking mode analysis on an extracted section from the mid-thickness of the LCD1 specimen, further metallurgical analysis was carried out on the fracture surface of the LCD1 specimen and the results are shown in Fig. 7. The EDM starter crack region, CCG region, FCG region and fast fracture region (i.e. associated with the specimen break open) can be observed on the fracture surface. As seen in this figure, intergranular and transgranular cracking modes can be observed on the fracture surface in the CCG and FCG zones, respectively. Additional SEM analysis, with higher magnification, was performed in the creep damage region where the fatigue crack starts to propagate. For this purpose, SEM analysis was conducted in through thickness direction at the end of the creep crack region and also after 1 mm of fatigue crack propagation. The SEM images captured in the transition region (i.e. early stage FCG region in the presence of creep damage) clearly demonstrate a change-over from intergranular to transgranular cracking mode at the beginning of the FCG region. This observation confirms that an interaction occurs between intergranular and transgranular failure mechanisms in the transition region. Another important observation from SEM analysis on the fracture surface after 1 mm of FCG is that although the dominant cracking mode is transgranular under fatigue loading conditions, some intergranular microcracks can be clearly observed along the grain boundaries as a result of creep damage. This implies that the existence of microcracks ahead of the initial fatigue crack tip would influence the subsequent FCG behaviour of the material.

6. Discussion

Comparison of the FCG trends between the LCD specimens and the PC material state reveals the influence of prior creep damage on subsequent fatigue cracking behaviour of the material. Fig. 5 shows that in the absence of significant plasticity (due to the material pre-straining thus hardening) the creep damage, which is formed in a confined region ahead of the crack tip in LCD specimens, results in a lower FCG trend compared to the material with no creep damage. Also seen in Fig. 5 is that towards the end of the tests on LCD specimens, the *da/dN* values converge towards those obtained from the material without creep damage. The observed FCG reduction in the presence of creep damage can be discussed in terms of the material degradation and microstructural changes as explained below:

(a) Creep strain effects on fatigue cracking behaviour: Under creep loading conditions, a pre-existing crack starts to propagate

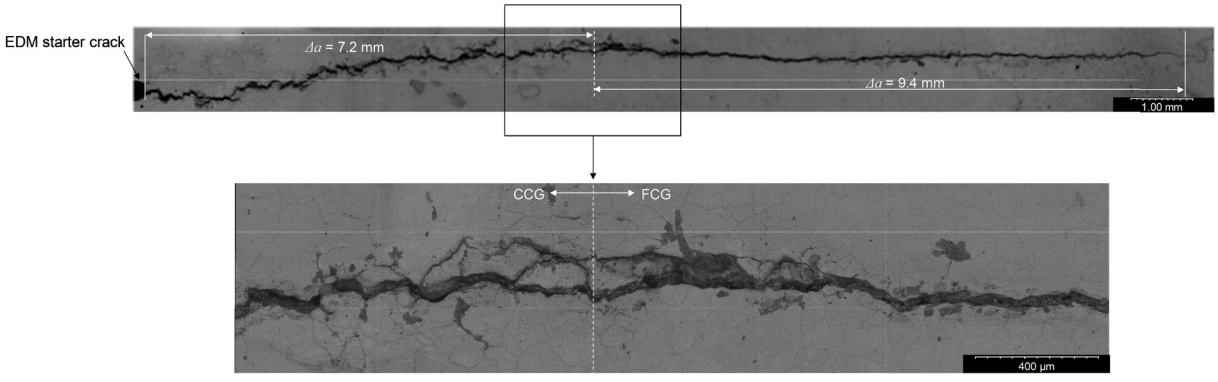

Fig. 6. The intergranular creep cracking mode and transgranular fatigue cracking mode in LCD1 specimen.

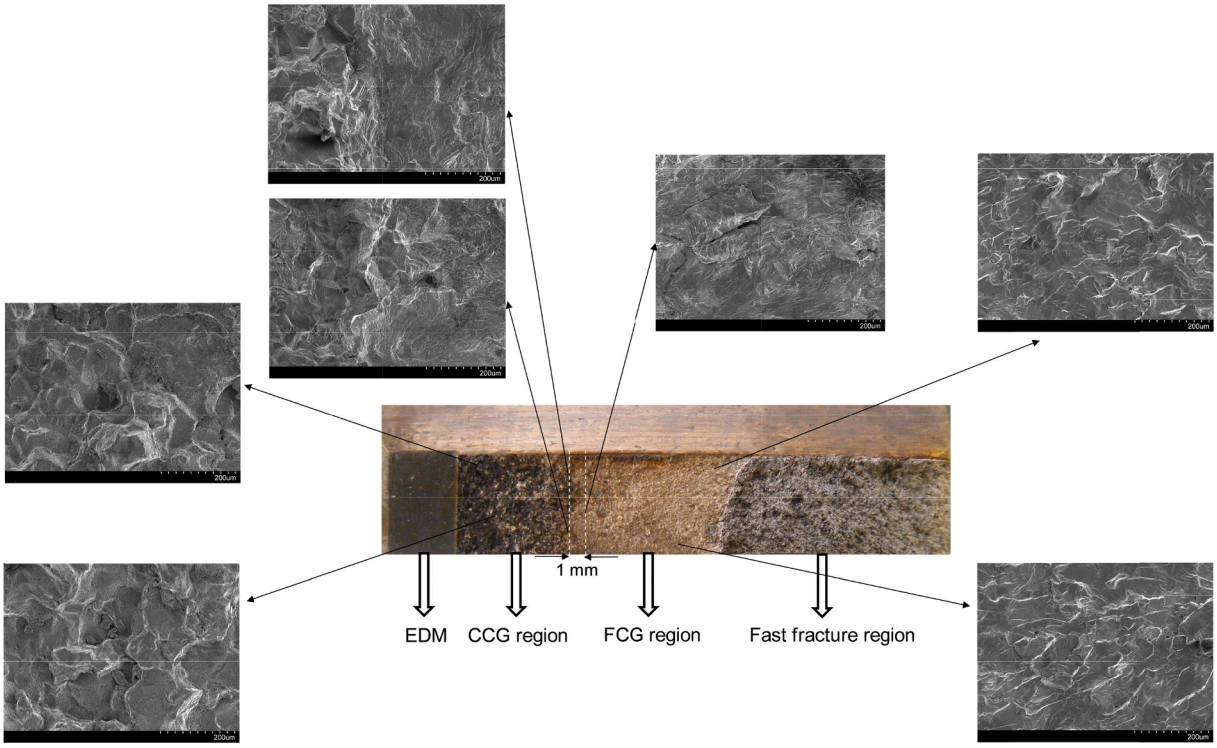

Fig. 7. SEM analysis of the fracture surface on LCD1 specimen.

when sufficient level of creep damage builds up ahead of the crack tip. When a creep crack starts to propagate, a widespread creep deformation region forms ahead of the crack tip and this condition is referred to as steady state CCG. Under steady state creep loading conditions, the stress and strain rate distribution fields can be described as a function of creep fracture mechanics parameter, C^*, using [35]:

$$\frac{\sigma_{ij}}{\sigma_0} = \left[\frac{C^*}{\dot{\varepsilon}_0 \sigma_0 I_n r}\right]^{\frac{1}{n+1}} \widetilde{\sigma}_{ij}(\theta; n) \tag{7}$$

$$\frac{\dot{\varepsilon}_{ij}}{\dot{\varepsilon}_0} = \left[\frac{C^*}{\dot{\varepsilon}_0 \sigma_0 I_n r}\right]^{\frac{n}{n+1}} \widetilde{\varepsilon}_{ij}(\theta; n) \tag{8}$$

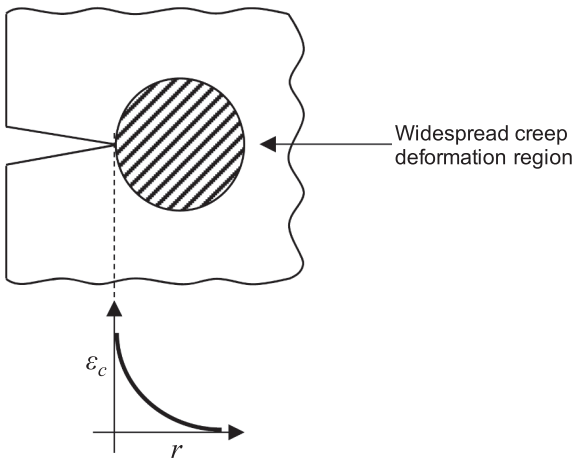

Fig. 8. Schematic illustration of the creep strain distribution ahead of the crack tip.

where σ_{ij} and $\dot{\varepsilon}_{ij}$ are the stress and strain rate tensors, respectively, σ_0 is the normalising stress, $\dot{\varepsilon}_0$ is the normalising strain rate, I_n is a non-dimensional constant, r is the radial distance from the crack tip, n is the power-law creep stress exponent, θ is the crack tip angle, and $\widetilde{\sigma}_{ij}(\theta;n)$ and $\widetilde{\varepsilon}_{ij}(\theta;n)$ are non-dimensional stress and strain values, respectively. The C^* parameter in Eqs. (7) and (8) can be experimentally calculated using [21]:

$$C^* = \frac{P\dot{\Delta}}{B_n(W-a)}H\eta \tag{9}$$

where P is the applied load, $\dot{\Delta}$ is the LLD rate, B_n is the net thickness between the side-grooves, W is the specimen width, a is the crack length, and H and η are geometry dependent constants. For a C(T) specimen with the normalised crack length in the valid range specified in ASTM E1457 standard, $H = n/(n+1)$ (where n is the power-law creep stress exponent) and $\eta = 2.2$ [19].

In Eqs. (7) and (8), σ_0, $\dot{\varepsilon}_0$, I_n and n, which are material properties/constants, remain unchanged throughout the CCG process. Moreover, it can be seen in Eq. (9) that in a given material and for a fixed crack length and loading condition the C^* parameter would remain constant. Therefore, at the end of the CCG tests on LCD specimens the local stress and creep strain rate (hence creep strain for a given time) will be inversely proportional to the distance from the crack tip. This means that at the crack tip, where r tends to zero, the local stress value will be infinitely high which results in the greatest level of local creep strain whilst both stress and creep deformation gradually reduce as the distance from the crack tip increases. The creep strain, ε_c, distribution in the widespread creep deformation region ahead of the crack tip has been schematically illustrated in Fig. 8. This figure shows that at the end of the CCG process a permanently deformed region is created ahead of the crack tip, which includes progressively reducing levels of creep strain. On the other hand, in the region sufficiently away from the crack tip (i.e. with large enough value of r) where there is no widespread creep deformation, the material has the same response as the bulk material without any creep pre-strain.

It has been shown by various researchers that a plastic zone size ahead of the crack tip significantly decelerates the FCG behaviour of engineering materials [34,36,37]. Knowing that creep deformation is analogous to plasticity, and they are both permanent deformations which harden the material [13], this suggests that the widespread creep deformation zone in LCD specimens would result in decelerated FCG rates which is consistent with the trends observed in Fig. 5. Moreover, Fig. 8 suggests that within the creep deformation zone, a gradual reduction in the creep strain level would result in a progressive increase in the FCG trend and when the crack advances and is located outside the creep deformation region the FCG rates would be the same as the material without any creep damage. This is in complete agreement with the FCG trends observed in specimens with and without creep damage which were shown in Fig. 5. It is worth noting that while the qualitative analysis of the local creep strain effects on the subsequent fatigue cracking behaviour of the material sufficiently explains and justifies the obtained results from the present study, a more detailed quantitative analysis will be conducted using finite element simulations in future work to evaluate the creep zone size and the influencing factors on formation of the local creep strain, and investigate their correlation with the extent of reductions in subsequent low temperature FCG rates.

(b) The effect of change-over in the cracking mode on the fatigue cracking behaviour: As seen in Fig. 6, a transition from intergranular to transgranular cracking mode occurs when the loading condition changes from creep to fatigue. Also, it was observed in Fig. 7 that intergranular voids and microcracks are formed ahead of the crack tip as a result of the CCG process. The microstructural creep damage, in the shape of voids and microcracks, which is formed within the widespread creep deformation region ahead of the crack tip, is schematically illustrated in Fig. 9. While the fatigue crack tends to follow a straight line normal to the applied loading direction, Fig. 9 shows that the existence of voids and microcracks along the grain boundaries can introduce local stress concentrations which would deviate the fatigue crack from its preferred direction. This condition will be more critical when the existing macrocrack tip (i.e. main crack) at the end of the CCG process is oriented along grain boundaries with large angles with respect to the preferred fatigue crack propagation direction along the specimen symmetry line (i.e. normal to the applied loading direction). Therefore, while the creep strain ahead of the crack tip decelerates the FCG rates, further delays at the early stages of the FCG process can occur due to the resistance of the microcracks against the change-over in the cracking mode from intergranular to transgranular. These two effects in combination describe the lower FCG rates observed in LCD samples shown in Fig. 5 compared to the material without any creep damage (i.e. PC material state).

7. Conclusions

Creep damage, local to the crack tip, was introduced into C(T) specimens made of 316H SS by interrupting CCG tests at 550 °C. To limit the extent of plasticity ahead of the crack tip in CCG tests, the material was uniformly pre-strained to 8% compressive plastic strain at room temperature prior to specimen manufacture, thus hardening the material. Room temperature FCG tests were performed on the AR, PC and LCD specimens under the load ratio of $R = 0.1$ and frequency of $f = 10$ Hz. The plastic pre-straining process was found to have insignificant effects on the FCG behaviour of the material at room temperature, though slightly lower trends were observed in the PC material compared to the AR material. Comparison of the LCD specimens with the PC material showed that creep damage reduces the FCG trend and the FCG rates in LCD specimens converged with the PC material only when the crack tip was located outside the initial creep damage zone. Further investigations showed that the reduced FCG trend in the LCD specimens is due to the formation of a creep pre-strain zone ahead of the crack tip. The extend of creep strain gradually reduces as the distance from the crack tip increases, hence why the FCG trends from the LCD specimens get closer to the PC material as the crack advances. Moreover, the metallurgical examinations demonstrated that the change-over from intergranular CCG to transgranular FCG can cause further delay in the crack propagation process, particularly in the presence of intergranular voids and microcracks in the creep damage zone which can

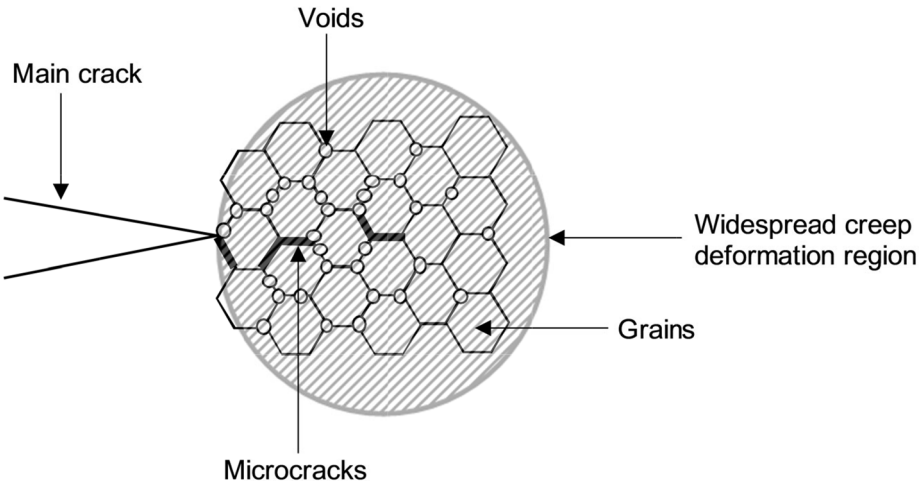

Fig. 9. Microstructural damage in the widespread creep deformation region ahead of the crack tip.

deviate the fatigue crack under cyclic loading conditions. Overall, the results confirm that creep damage, when introduced to a confined region ahead of the crack tip, reduces da/dN for a given value of ΔK due to the mechanical (i.e. local creep pre-straining) and microstructural (i.e. intergranular voids and microcracks) reasons demonstrated in this study. The presented results make significant contribution to knowledge and facilitate the enhancement of the structural integrity assessment procedures for high temperature pressure vessels, particularly the aged steam headers in AGRs.

CRediT authorship contribution statement

Ali Mehmanparast: Writing – original draft, Methodology, Formal analysis, Conceptualization. **Kamran Nikbin:** Writing – review & editing, Investigation, Conceptualization.

Declaration of Competing Interest

The authors declare that they have no known competing financial interests or personal relationships that could have appeared to influence the work reported in this paper.

Acknowledgments

The author would like to thank EDF Energy for supporting this research.

References

[1] Mehmanparast A, Davies CM, Webster GA, Nikbin KM. Creep crack growth rate predictions in 316H steel using stress dependent creep ductility. Mater High Temp 2014;31(1):84–94.
[2] Mehmanparast A, Davies CM, Dean DW, Nikbin KM. The influence of pre-compression on the creep deformation and failure behaviour of Type 316H stainless steel. Eng Fract Mech 2013;110:52–67.
[3] Mehmanparast A, Davies CM, Dean DW, Nikbin K. Material pre-conditioning effects on the creep behaviour of 316H stainless steel. Int J Press Vessel Pip 2013;108:88–93.
[4] Mehmanparast A, Davies CM, Dean DW, Nikbin K. Effects of plastic pre-straining level on the creep deformation, crack initiation and growth behaviour of 316H stainless steel. Int J Press Vessel Pip 2016;141:1–10.
[5] Mehmanparast A, Davies CM, Dean DW, Nikbin KM. Plastic pre-compression and creep damage effects on the fracture toughness behaviour of Type 316H stainless steel. Eng Fract Mech 2014;131:26–37.
[6] Colin J, Fatemi A, and Taheri S. "Fatigue behavior of stainless steel 304L including strain hardening, prestraining, and mean stress effects," 2010.
[7] Srinivasan VS, Sandhya R, Valsan M, Rao KBS, Mannan SL. Comparative evaluation of strain controlled low cycle fatigue behaviour of solution annealed and prior cold worked 316L (N) stainless steel. Int J Fatigue 2004;26(12):1295–302.
[8] Radhakrishnan VM, Baburamani PS. An investigation of the effect of pre-straining on fatigue crack growth. Mater Sci Eng 1975;17(2):283–8.
[9] Radhakrishnan VM, Baburamani PS. Initiation and propagation of fatigue crack in pre-strained material. Int J Fract 1976;12(3):369–80.
[10] Melnikov BE. Effect of prestrain on fatigue crack growth in low-carbon steel. Mag Civ Eng 2011;3:71–4.
[11] Ikematsu K, Mishima T, Kang M, Aono Y, Noguchi H, Neu R, et al. Effect of Prestrain on Fatigue Crack Growth of Age-Hardened Al 6061-T6. J ASTM Int 2008;5(8):101549.
[12] Mehmanparast A, Davies CM. The influence of inelastic pre-straining on fracture toughness behaviour of Type 316H stainless steel. Eng Fract Mech 2018;188:112–25.
[13] Mehmanparast A, Davies CM, Dean DW, and Nikbin KM. "The influence of inelastic damage on tensile deformation and creep crack growth behaviour of type 316H stainless steel," in Pressure Vessels and Piping Conference, 2013, vol. 55706, p. V06AT06A044.
[14] Shinya N, Kyono J, Kushima H, Yokoi S. Effect of Creep Damage on Fatigue Life of Cr–Mo–V Steel. Trans Natl Res Inst Met (Jpn) 1987;29(2):115–23.
[15] Gan D. Tensile and fracture properties of type 316 stainless steel after creep. Metall Trans A 1982;13(12):2155–63.

[16] Albertini C. and Montagnani M. "Strain-rate dependence of residual strength and ductility of AISI 316 stainless steel after creep, fatigue and irradiation," 1987.
[17] Anderson TL. Fracture mechanics: fundamentals and applications. CRC Press; 2017.
[18] ASTM-E647-15, Standard test method for measurement of fatigue crack growth rates. ASTM international, 2015.
[19] ASTM-E1457-19, "Standard Test Method for Measurement of Creep Crack Growth Times in Metals," 2019.
[20] Tarnowski KM, Nikbin KM, Dean DW, Davies CM. Improvements in the measurement of creep crack initiation and growth using potential drop. Int J Solids Struct 2018;134:229–48.
[21] Webster GA, Ainsworth RA. High temperature component life assessment. Springer Science & Business Media; 2013.
[22] ESIS-P2–92, "Procedure for determining the fracture behaviour of materials," Eur. Struct. Integr. Soc., 1992.
[23] ASTM-1820-18, "Standard Test Method for Measurement of Fracture Toughness," Annu. B. Stand, vol. 3, no. 1, 2018.
[24] Dean DW, Gladwin DN. Creep crack growth behaviour of Type 316H steels and proposed modifications to standard testing and analysis methods. Int J Press Vessel Pip 2007;84(6):378–95.
[25] P. Paris and F. Erdogan, "A critical analysis of crack propagation laws," 1963.
[26] Paris PC. A rational analytic theory of fatigue. trend Eng 1961;13:9.
[27] Mehmanparast A, Brennan F, Tavares I. Fatigue crack growth rates for offshore wind monopile weldments in air and seawater: SLIC inter-laboratory test results. Mater Des 2017;114:494–504.
[28] Tada H, Paris PC, Irwin GR. The stress analysis of cracks. Handbook, Del Res. Corp. 1973;34.
[29] Ohta A, Suzuki N, Maeda Y. Unique fatigue threshold and growth properties of welded joints in a tensile residual stress field. Int J Fatigue 1997;19(93):303–10.
[30] Benachour M, Benachour N, Benguediab M. Fatigue crack initiation and propagation through residual stress field. Int J Mech Mechatronics Eng 2012;6(11):2470–4.
[31] Panasyuk VV, Andreykiv OY, Ritchie RO, Darchuk OI. Estimation of the effects of plasticity and resulting crack closure during small fatigue crack growth. Int J Fract 2001;107(2):99–115.
[32] Edwards L, Zhang YH. Investigation of small fatigue cracks—II. A plasticity based model of small fatigue crack growth. Acta Metall Mater 1994;42(4):1423–31.
[33] Zhang J-Z, Zhang J-Z, Du SY. Elastic–plastic finite element analysis and experimental study of short and long fatigue crack growth. Eng Fract Mech 2001;68(14):1591–605.
[34] Solanki K, Daniewicz SR, Newman JC. Finite element analysis of plasticity-induced fatigue crack closure: an overview. Eng Fract Mech 2004;71(2):149–71. https://doi.org/10.1016/S0013-7944(03)00099-7.
[35] Riedel H. and Rice JR. "Tensile cracks in creeping solids." 1980. doi: 10.1520/stp36967s.
[36] de Matos PFP, Nowell D. Experimental and numerical investigation of thickness effects in plasticity-induced fatigue crack closure. Int J Fatigue 2009;31(11-12):1795–804.
[37] Rice JR. "Mechanics of crack tip deformation and extension by fatigue". Fatigue Crack Propagation, ASTM STP 415, Am. Soc. Testing Mats. 1967.